Available online at www.sciencedirect.com

SciVerse ScienceDirect

Ceramics International 39 (2013) 8393–8400

CERAMICS INTERNATIONAL

www.elsevier.com/locate/ceramint

Investigations on phase constitution, mechanical properties and hydration kinetics of aluminous cements containing magnesium aluminate spinel

Jin-hong Li*, Bi-ya Cai, Wu-wei Feng, Yu-qin Liu, Hong-wen Ma

National Laboratory of Mineral Materials, China University of Geosciences, Beijing 100083, China

Received 27 February 2013; received in revised form 7 April 2013; accepted 7 April 2013
Available online 16 April 2013

Abstract

Aluminous cement containing magnesium aluminate (ACMA) spinel was prepared in situ by sintering mixtures of limestone, magnesia and bauxite. The phase constitution, micro-morphology, and hydration kinetics of ACMA were investigated by X-ray diffraction (XRD), scanning electron microscope (SEM) and isothermal calorimeter measurements, respectively. Magnesium aluminate (MA) spinel, calcium monoaluminate (CA) and calcium bialuminate (CA_2) are the primary phases of the obtained ACMA. In addition, trace amount of calcium silicoaluminate (C_2AS) and residual alumina (Al_2O_3) were detected. MA, mainly exists in the form of octahedron on the order of 2–5 μm and forms agglomerates with the tabular or flaky-shaped CA in the clinker. The compressive strength of the ACMA castables increased remarkably as a function of CA content. The measurement of hydration heat demonstrated a five stage hydration process, namely, pre-induction, induction, acceleration, deceleration and stabilization. The *N* value was calculated to be lower than 1 in acceleration stage which indicates a nucleation controlled hydration process. On the other hand, it was higher than 1 in stabilization stage showing a diffusion controlled process.

Keywords: Magnesium aluminate spinel; Aluminous cement; Phase constitution; Mechanical properties; Hydration kinetics

1. Introduction

Refractory castables containing aluminous cements with the addition of synthetic spinel have numerous applications in the metallurgy, geochemistry, ceramic, cement, and glass industries, due to their excellent properties, such as high melting point, low thermal expansion, considerable hardness, high resistance to chemical attack, favorable chemical stability, and good thermal spalling [1,2]. Magnesium aluminate (MA) is extensively used in high performance refractory castables because of its desirable combination of mechanical, chemical and thermal properties both at ambient and elevated temperatures [3–5]. The refractoriness of the high alumina cements mainly consisting of calcium aluminate (CA) and calcium bialuminate (CA_2) can be increased substantially, without affecting their compressive strength, when CaO in the cement clinker is partially substituted by MgO due to the formation of MA [6,7].

Dolomite and alumina are the most popular raw materials used to fabricate aluminous cement containing magnesium aluminate (ACMA) spinel. Nagy [6] prepared calcium aluminate cements containing MA spinel by using Egyptian dolomite and active alumina, which exhibited a compromise between considerable strength and higher refractoriness. When 10% of such cements were added to refractory grade magnesia aggregate, with 0.1% Li_2CO_3 as a strength modifier, the hot-strength and thermal shock resistance of refractory castable bodies was improved. Xiao's report [8] also showed that ACMA has good cold bonding strength, higher refractoriness and good corrosion resistance, compared with aluminous cement. Nevertheless, it was hard to control the proportion of MA and CA phases in end products due to the relatively fixed contents of CaO and MgO in dolomite.

Although many works have been done on the strength, high refractoriness and anti-erosion ability of ACMA, hydration kinetics is still kept unknown. The purpose of this work is to investigate a new series of tunable mineralogical phase, ACMA, by sintering mixtures of limestone, magnesia and bauxite, in order to well understand and improve the performances of ACMA. The phase constitution, micro-morphology,

*Corresponding author. Tel.: +86 010 82323201.
E-mail address: jinhong@cugb.edu.cn (J.-h. Li).

0272-8842/$ - see front matter
http://dx.doi.org/10.1016/j.ceramint.2013.04.020

Table 1
Chemical compositions of the raw materials (wt%).

Raw materials	SiO_2	Al_2O_3	TFe_2O_3/FeO	CaO	MgO	K_2O	Na_2O	TiO_2	MnO	P_2O_5	Loss	Total
Limestone	2.82	0.22	0.01	53.52	0.47	0.05	0.02	0.03	–	–	43.08	100.22
Magnesia	3.25	0.94	1.06	1.81	91.18	0.02	0.04	0.03	0.06	0.09	1.02	99.50
Bauxite	4.91	88.67	0.91	0.33	1.05	0.079	0.008	3.55	–	–	0.029	99.54

TFe_2O_3/FeO = total amount of Fe_2O_3 and FeO.

Table 2
The designed phase constitution of ACMA and composition of raw materials (wt%).

Sample	Phase constitution					Composition of raw materials		
	CA	MA	CA_2	C_2AS	C_2F	Limestone	Magnesia	Bauxite
CA-40	40	50	4.7	5	0.3	25.90	11.86	61.95
CA-48	48	42	4.7	5	0.3	29.77	9.63	60.59
CA-56	56	34	4.7	5	0.3	33.50	7.48	59.00
CA-64	64	26	4.7	5	0.3	37.13	5.40	57.46

CA: $CaO \cdot Al_2O_3$; MA: $MgO \cdot Al_2O_3$; CA_2: $CaO \cdot 2Al_2O_3$; C_2AS: $2CaO \cdot Al_2O_3 \cdot SiO_2$; C_2F:$2CaO \cdot Fe_2O_3$.

mechanical properties, and hydration kinetics of the obtained clinker and castables were studied.

2. Experimental

2.1. Starting materials

Local limestone (source of CaO), light burnt magnesia (source of MgO) and calcined bauxite (source of Al_2O_3) were employed for preparation of ACMA. The chemical compositions of the three raw materials are given in Table 1.

2.2. Preparation of cement compositions

Three raw materials were mixed by the designed composition (Table 2) and ball milled until the particle size was reduced below 0.355 mm. The mixtures were pressed into pellet using cold isostatic pressure of 30–50 MPa, and then dried at 110 °C followed by firing at 1400 °C for 3 h. The resulting sintered clinkers were crushed and finely ground and sieved to obtain fine cement powder.

2.3. Characterization methods

The obtained clinkers and hydration product were characterized by X-ray diffraction (XRD, Model Philips X) and scanning electron microscopy (SEM, Model FEI Quanta 200 F). The XRD measurement was operated at 40 kV and 40 mA with nickel filtered Cu Kα radiation. Compressive strength of the castables was measured using computer-controlled hydraulic universal test (Model WEW-50). All samples were poured using cubic molds ($20 \times 20 \times 20$ mm^3) after estimating the compact particle packing. These specimens were then air-dried for 24 h, followed by curing in humidity box for 1, 3, 7 or 28 d (temperature: 20 ± 0.5 °C, relative humidity: 95%). During hydration test, a commercial Lafarge cement labeled SECAR68, produced by Kerneos (China) aluminate technology Co. Ltd., was used as a reference. Hydration heat emission rate and quantity of cement samples were measured by isothermal calorimeter, marked as TONI. The Ca^{2+} ions concentrations, conductivity rates and pH values were measured by 721-type spectrophotometer, PHS-2C type pH meter, and DDS2 IIA type conductivity meter, respectively.

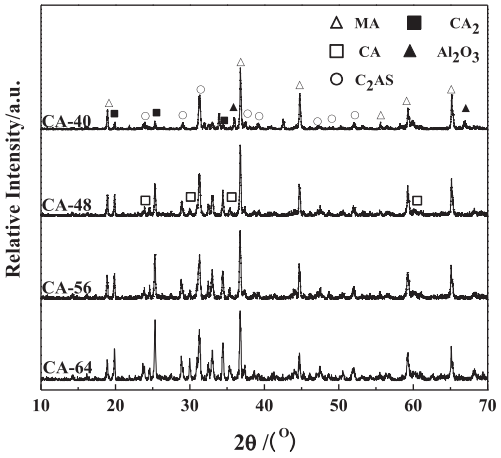

Fig. 1. XRD patterns of the ACMA clinkers. (CA: $CaO \cdot Al_2O_3$; MA: $MgO \cdot Al_2O_3$; CA_2: $CaO \cdot 2Al_2O_3$; C_2AS: $2CaO \cdot Al_2O_3 \cdot SiO_2$).

3. Results and discussions

3.1. Phase composition and micro-morphology of the prepared clinker

XRD patterns of the clinkers with different contents of magnesium aluminate (MA) spinel are shown in Fig. 1. As seen in the pattern of CA-48 which contains 42 wt% MA, residual Al_2O_3 could not be detected. Secondary dominant phase was observed to be calcium aluminate (CA). When the content of MA is below 42 wt%, CA, MA, calcium bialuminate (CA_2) and calcium silicoaluminate (C_2AS) constitute the major phases of the cement clinkers and the intensity of MA peaks is strong in all patterns. Moreover, there is a significant increase in the intensity of CA, CA_2 and C_2AS peaks as the content of MA decreases from 42 wt% to 26 wt%.

The micro-morphology of the ACMA clinkers is shown in Fig. 2. As seen in Fig. 2a and b, CA-48 microstructure is mainly composed of octahedron-shaped MA crystals between 2 and 5 μm and large tabular CA crystals in the range of 20–40 μm. In the

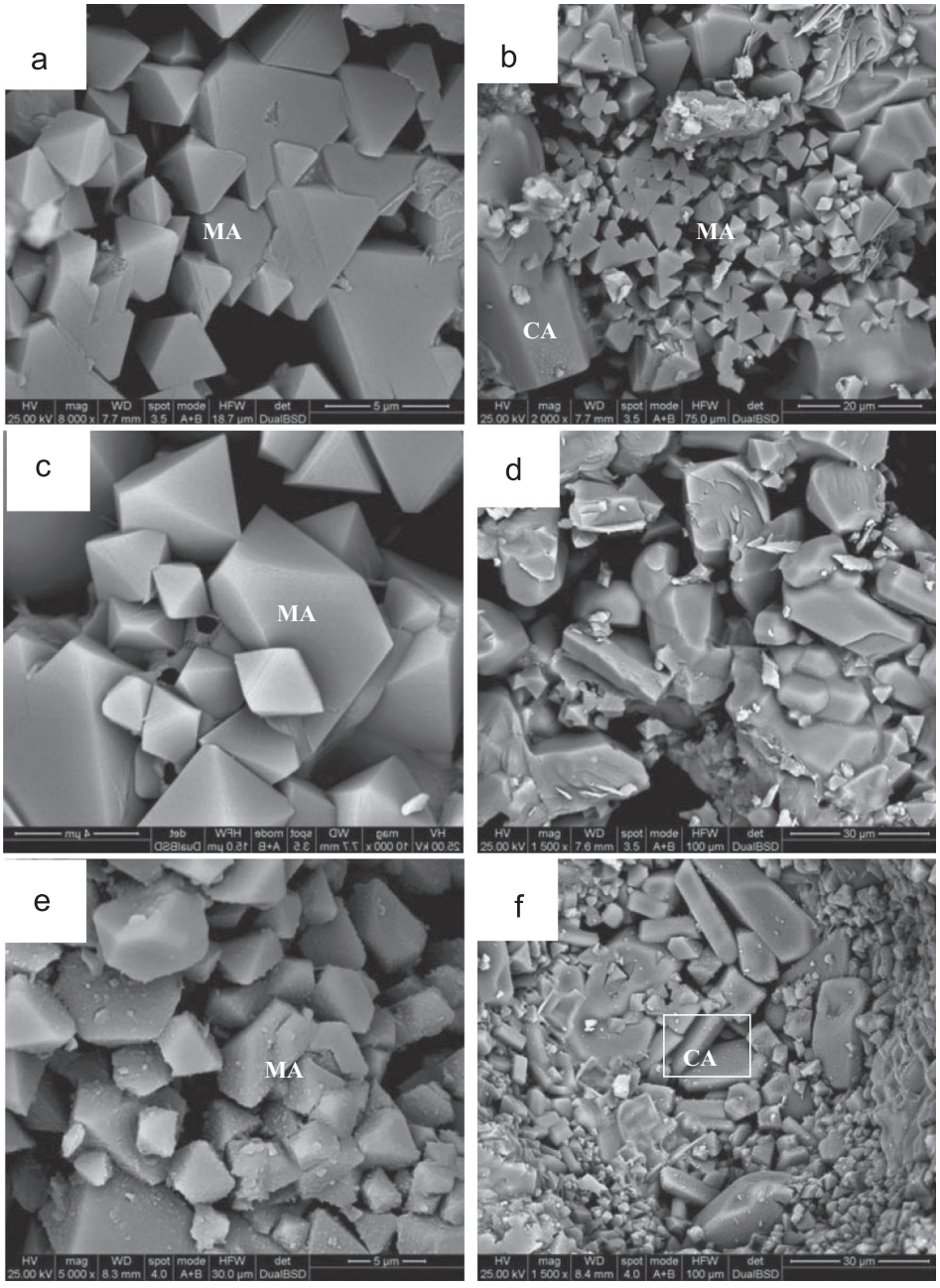

Fig. 2. SEM photographs of the ACMA clinkers with different MA contents: ((a)–(c) CA-48; (d) CA-56; (e), (f) CA-64).

CA-56 microstructure (Fig. 2d), MA grains with smaller crystal size and good crystallization are observed in the intergranular boundary between the irregular tabular-shaped or puncheon-shaped CA crystals.

The MA crystals, about 2–5 μm in size, are observed in the specimen CA-64 (Fig. 2e) with O 46.28 at%, Mg 14.73 at%, Al 37.05 at.%, Ca 0.80 at%, Fe 1.15 at% according to EDS measurement. Besides, some whiskers with a high aspect ratio are also observed. The EDS spectrum displays that the selected crystals are consisted of 38.23 at% O, 47.09 at% Al, 13.24 at% Ca and 1.43 at% Fe, indicating that CA is the main phase in the selected area. The CA and MA crystals forms agglomerates and dispersed throughout the C-64 microstrcuture (Fig. 2f).

Backscattered electron images of the CA-56 clinker (Fig. 3a) reveal the presence of agglomeration consisting of grayish-black MA grains, light-gray CA grains, and a small amount of white gray CA_2 grains. Meanwhile, as shown in Fig. 3b, only a few MA and CA_2 grains exist among the CA crystals in the specimen CA-64.

3.2. Phase transformation and compressive strength of obtained cements during hydration

Fig. 4 shows the XRD patterns of CA-64 and SECAR68 samples at different hydration stages. The MA is not a hydraulic mineral which is nonreactive in the hydration process, as seen from

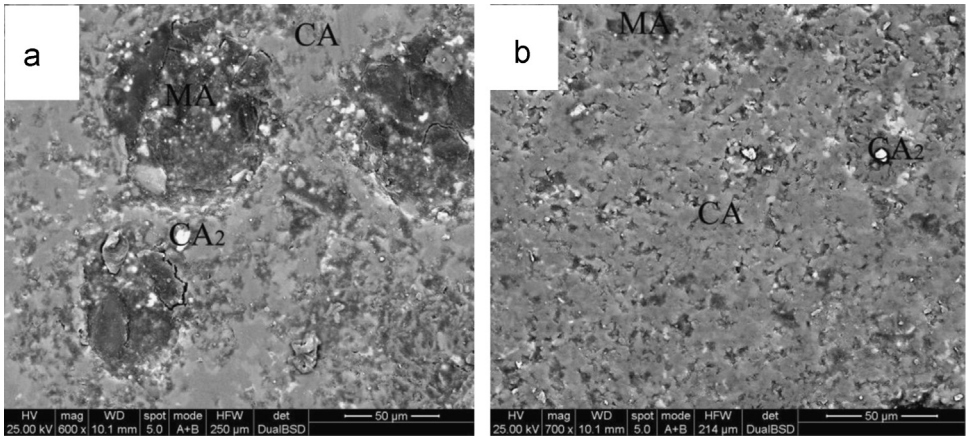

Fig. 3. Backscattered electron images of CA-56 (a) and CA-64 (b) clinkers.

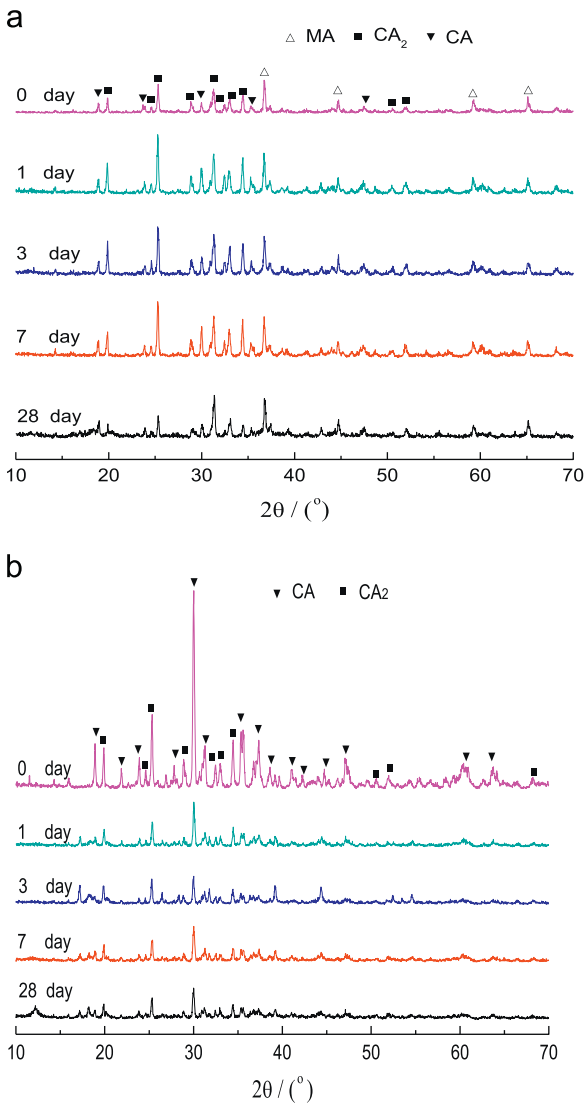

Fig. 4. The XRD patterns of CA-64 (a) and SECAR68 (b) cements at different curing time.

the unchanged peak intensity of MA shown in Fig. 4a. The peak intensity of CA_2 and CA phases in CA-64 sample do not change obviously during the first 7 days, while it declines significantly

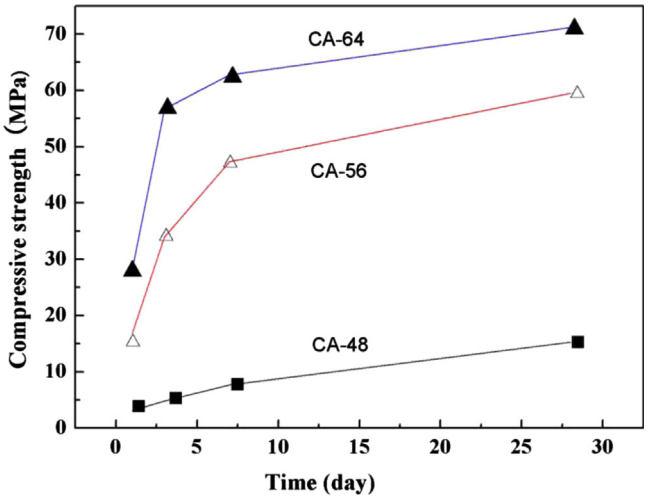

Fig. 5. Compressive strength of various ACMA specimens at different curing time.

in SECAR68 cement for a 1 day hydration. MA is not hydration-reactive owing to its stability and also limits the hydration reaction of CA_2 and CA phases to some extent. Therefore, the hydration rate of ACMA is slower than that of the Lafarge cement. The XRD patterns of the two cements after 28 days hydration indicate that CA_2 and CA do not react completely.

Fig. 5 illustrates the compressive strength of the specimens as a function of curing time. At the same curing time, the compressive strength increases significantly with decrease of the MA content in the cement clinkers, which is attributed to the increased hydration. Due to the lack of hydraulicity of MA phase, CA and CA_2 phases are the primary factors in the processes of hydration. Furthermore, a sharp increase in compressive strength can be observed in the all specimens before curing for 3 days hydration. Afterwards the increase of compressive strength slow down due to the formation of C_2AH_8 from CAH_{10}. Note that C_2AH_8 has a faster hardening speed and a higher hardness compared to CAH_{10} [9]. The highest compressive strength of 71.2 MPa is obtained in the specimen CA-64 after 28 days curing.

3.3. Hydration heat and kinetics

The main phases in CA-64 cement are MA, CA_2 and CA. MA is not a hydraulic mineral and is nonreactive during hydration process. CA_2 and CA are the main phases of SECAR68 cement. Therefore, the main hydration reactions in above two cements are the hydration reactions of CA and CA_2 phases:

$$3CA + 12H \rightarrow C_3AH_6 + 2AH_3 \quad (1)$$

$$3CA_2 + 21H \rightarrow C_3AH_6 + 5AH_3 \quad (2)$$

Isothermal calorimeter was used to measure the hydration heat emission rate and quantity of CA-64 and SECAR68 cements at 25 °C, as shown in Fig. 6. The hydration processes of the two cements could be classified to five stages according to the calculation: pre-induction (A), induction (B), acceleration (C), deceleration (D) and stabilization (E).

By applying the ToniDCA V2.0.0 of isothermal calorimeter software (abbreviated TONI), the values of Q_{max} were obtained. Knudsen [10] derived the cement hydration kinetics equation:

$$1/Q = 1/Q_{max} + t_{50}/Q_{max}(t-t_0) \quad (3)$$

where Q is hydration heat emission quantity, Q_{max} is the final hydration heat emission quantity, t is the time of hydration, t_0 is the time at the beginning of acceleration stage; and t_{50} is the time when half of the hydration reaction has completed.

The y-intercept of this linear equation is $1/Q_{max}$ as seen from the established linear relationship between $1/Q$ and $1/(t-t_0)$in Eq. (3). The correlation between $1/Q$ and $1/(t-t_0)$ for the two cements are shown in Fig. 7, the hydration kinetics equation for the CA-64 cement is $1/Q = 0.004128 + 0.0384/(t-t_0)$, with the correlation coefficient $R^2 = 0.9982$ and $Q_{max} = 242.25$ J/g. The hydration kinetics equation for the SECAR68 cement is $1/Q = 0.002930 + 0.0079/(t-t_0)$, with correlation coefficient $R^2 = 0.9981$ and $Q_{max} = 341.30$ J/g. The measured values of Q_{max} are slightly lower than the calculated one, due to the fact that the designed ratio of water was not enough to allow complete hydration of cement. The hydration heat of CA-64 cement is less than that of SECAR68 cement, which reduces the temperature difference between inside and outside concrete, and thus decreases the possibility of concrete cracking.

Sakai et al. [11] proposed a hydration kinetics equation for the cement:

$$[1-(1-\alpha)^{1/3}]^N = \kappa(t-t_0) \quad (4)$$

where α ($\alpha = Q/Q_{max}$) is the degree of hydration; N is a constant related to the reaction mechanism, if $0 < N < 1$, the hydration is controlled by nucleation reaction, if $N \geq 1$, the hydration is controlled by diffusion process; κ is a constant of

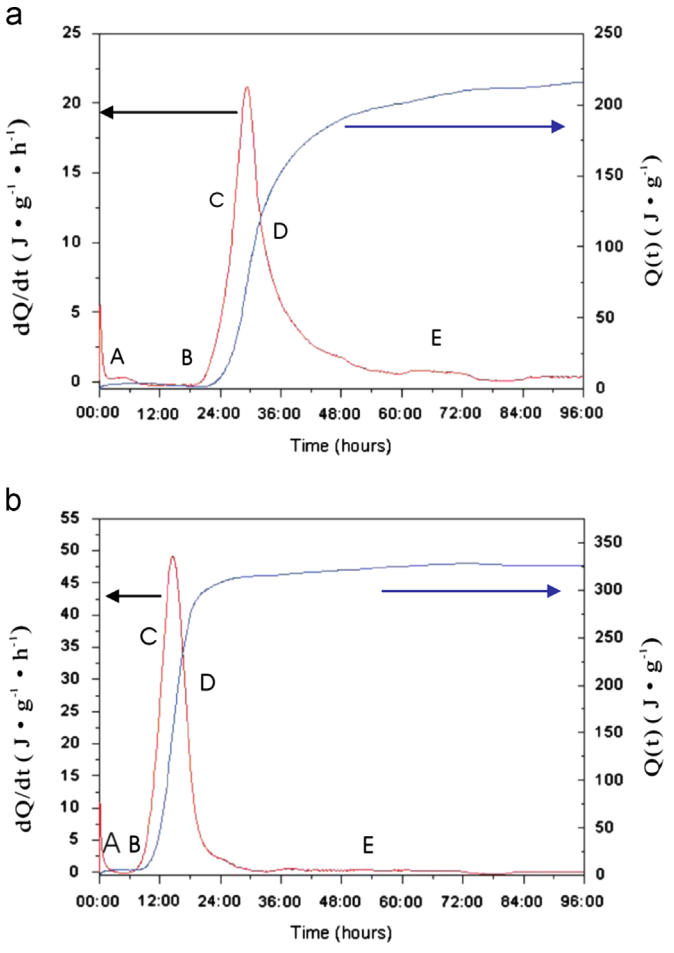

Fig. 6. Hydration heat emission rate and quantity of CA-64 (a) and SECAR68 (b) cements.

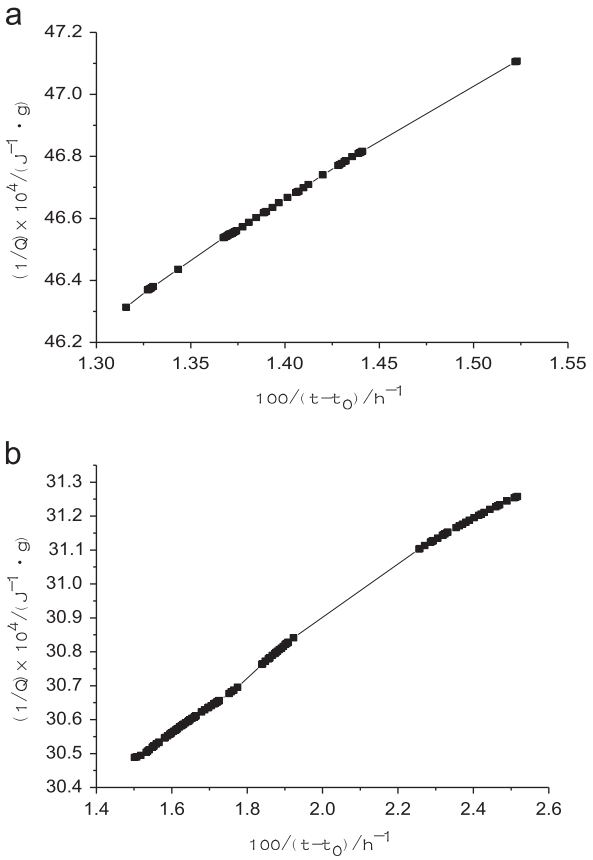

Fig. 7. Relationship between $1/Q$ and $1/(t-t_0)$ of hydrated CA-64 (a) and SECAR68 (b) cements.

reaction rate; t_0 is the starting time of acceleration stage; $t-t_0$ is the duration from t_0.

After taking logarithm of Eq. (4), the equation turns into

$$ln\left[1-(1-\alpha)^{1/3}\right] = \frac{1}{N}\ ln\kappa + \frac{1}{N}\ ln(t-t_0) \quad (5)$$

Fig. 8 shows the correlation between $\ln[1-(1-\alpha)^{1/3}]$ and $\ln(t-t_0)$, where the values of N and κ were obtained from the slope of curve and the y-intercept.

As shown in Fig. 8, linear-correlation governs the acceleration and stabilization stages for both cements, whereas nonlinear-correlation is dominant in the deceleration stage. Eq. (4) can explain the acceleration and stabilization stages for the two cements, however, is not suitable for deceleration stage.

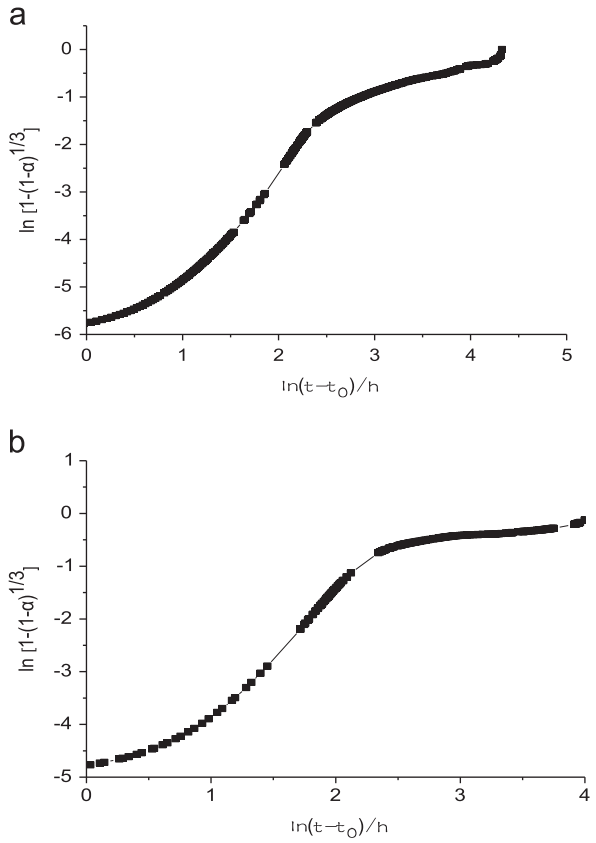

Fig. 8. Relationship between $\ln[1-(1-\alpha)^{1/3}]$ and $\ln(t-t_0)$ for the CA-64 (a) and SECAR68 (b) cements.

The parameters of hydration kinetics in acceleration and stabilization stages of the two cements were obtained by applying Eq. (4), as shown in Table 3. The N values in acceleration stage for both cements are lower than 1. Therefore, the main hydration reaction in acceleration stage is nucleation. The nucleation rate of SECAR68 cement is faster than that of CA-64 cement. The N values in stabilization stage for both cements are higher than 1, thus the major hydration reaction in stabilization stage is diffusion. The diffusion rate of SECAR68 cement is faster than that of CA-64. Comparing the κ values between acceleration stage and stabilization stage, the reaction rate in acceleration stage is faster than that of stabilization stage, therefore, the SECAR68 cement would have faster hydration reaction rate and higher early strength due to its faster nucleation rate in the acceleration stage.

Based on Arrhenius formula:

$$\kappa = e^{-E/RT} \quad (6)$$

where κ is a constant of reaction rate, E is apparent activation energy, R is molar gas constant, and T is thermodynamic temperature. The apparent activation energy in acceleration and stabilization stages for both cements are shown in Table 3. The E value of CA-64 cement is higher than that of SECAR68 cement, indicating the energy to break existing bonds and create new bonds of hydration products in CA-64 cement is larger than that in SECAR68 cement, which is consistent with their hydration rate.

Fig. 9 gives the soluble concentrations of Ca^{2+} ions, conductivity rates and pH values at different hydration stages for CA-64 and SECAR68 cements. The soluble concentration of Ca^{2+} ions of SECAR68 cement reaches maximum after 5 h hydration, indicating the dissolution of Ca^{2+} ions from CA and CA_2 in induction stage during hydration process. The soluble concentration of Ca^{2+} ions decreases dramatically beyond 10–15 h hydration, which illustrates that the soluble Ca^{2+} ions have reacted drastically and formed the hydration products during acceleration stage. The soluble concentration of Ca^{2+} ions declines slightly after 15 h, indicating the beginning of deceleration and stabilization stages. The soluble concentration of Ca^{2+} ions of CA-64 cement reaches its maximum after 11 h hydration, which is slower than that of SECAR68. This can be explained by the slower hydration rate in CA-64 cement. The soluble concentration of Ca^{2+} ions decreases from 11 h to 48 h, indicating the drastic reaction of the soluble Ca^{2+} ions

Table 3
Hydration kinetics parameters of CA-64 and SECAR68 cements.

Age	Parameter	CA-64	SECAR68
Acceleration	Time (h)	21–28	10–16
	N	0.5440	0.4091
	Constant of hydration rate, κ	2.702×10^{-2}	7.490×10^{-2}
	Apparent activation energy, E (kJ mol^{-1})	8.95	6.42
Stabilization	Time (h)	≥40	≥28
	N	1.9146	2.7894
	Constant of hydration rate, κ	9.422×10^{-3}	1.109×10^{-2}
	Apparent activation energy, E (kJ mol^{-1})	11.56	11.15

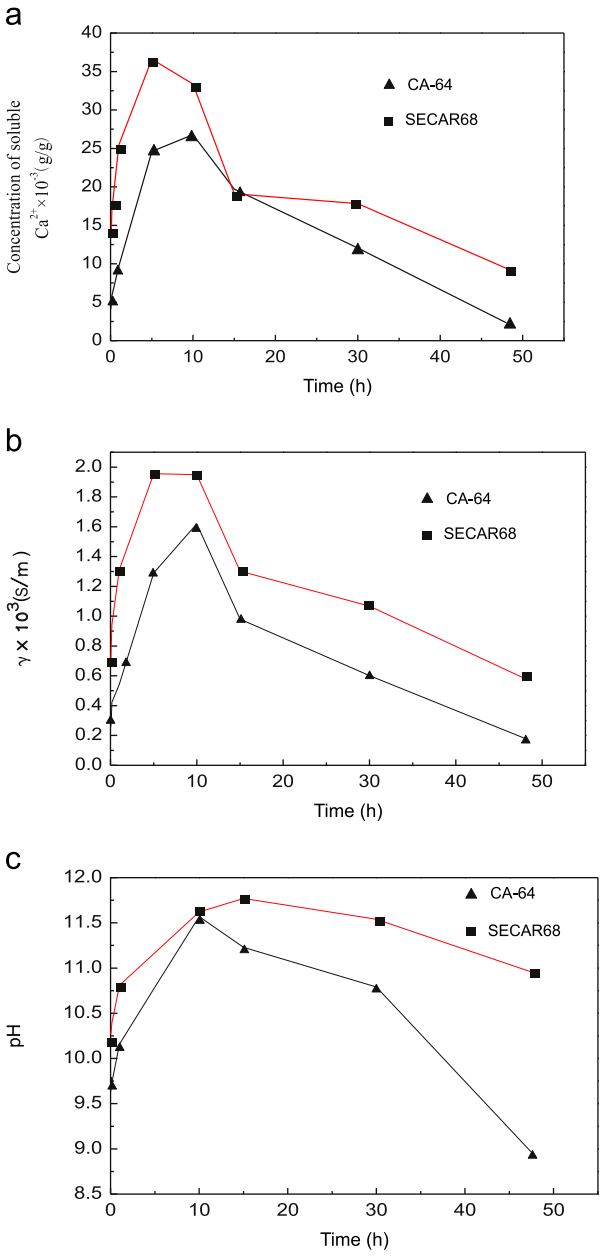

Fig. 9. The soluble concentrations of Ca^{2+} ion (a), conductivity rates (b), and pH values (c) for the CA-64 and SECAR68 cements during hydration.

during acceleration stage. The soluble concentration of Ca^{2+} ions of SECAR68 cement is always higher than that of CA-64 cement depending on the hydration rate. The variation trend of the conductivity rate is similar to that of soluble concentration of Ca^{2+} ions. The pH value of CA-64 cement are lower than that of SECAR68 at different hydration stages, and decreases to 8.8 after 48 h. Note that the lower pH value is beneficial to avoid alkali-aggregate reaction and enhanced durability.

4. Conclusions

A new phase-tunable aluminous cement containing magnesium aluminate spinel (ACMA) was prepared by sintering mixtures of limestone, magnesia and bauxite. The obtained ACMA cement was mainly composed of magnesium aluminate (MA) spinel, calcium monoaluminate (CA) and calcium bialuminate (CA_2), with trace amount of calcium silicoaluminate (C_2AS) and residual alumina (Al_2O_3). The octahedron-shaped MA crystals on the order of 2–5 μm and tabular or flaky-shaped CA in the range of 20–40 μm form agglomerates and disperse in the aluminous cements. MA plays a negative role on compressive strength of the hydrated castables.

Five stages exist in the hydration processes of ACMA and commercial aluminous cement (SECAR68), including pre-induction, induction, acceleration, deceleration and stabilization. In acceleration stage, the hydration of ACMA is controlled by nucleation reaction, and the hydration rate is slower than that of SECAR68. In stabilization stage, the hydration of ACMA is controlled by diffusion, and the hydration rate becomes slower. The MA-spinel is nonreactive in hydration process, and inhibits the hydration rate of CA and CA_2. The hydration heat of ACMA is less than that of SECAR68, which might be helpful to reduce the temperature difference between inside and outside of concrete and avoid concrete cracking.

A large amount of Ca^{2+} ions have dissolved out from CA and CA_2 in induction stage during the hydration process. At the beginning of acceleration stage, the soluble Ca^{2+} ions reach saturation. Afterwards, drastical reaction, accompanying generation of hydration products, results in the decreases of Ca^{2+} ions concentration. The concentration of Ca^{2+} ions declines slightly in deceleration and stabilization stages.

Acknowledgments

This project was supported by program for New Century Excellent Talents in University (NCET-08-828), the Fundamental Research Funds for the Central Universities (2011YXL003), and Research Fund of National Laboratory of Mineral Materials (no. A08002).

References

[1] A.H. De Aza, P. Pena, M.A. Rodriguez, R. Torrecillas, S.De Aza, New spinel-containing refractory cements, Journal of the European Ceramic Society 23 (2003) 737–744.
[2] L.A. Diaz, R. Torrecillas, F. Simonin, G. Fantozzi, Room temperature mechanical properties of high alumina refractory castables with spinel, periclase and dolomite additions, Journal of the European Ceramic Society 28 (2008) 2853–2858.
[3] S. Mukhopadhyay, P.K. Das Poddar, Effect of preformed and in situ spinels on microstructure and properties of a low cement refractory castable, Ceramics International 30 (2004) 369–380.
[4] Salah A. Abo-El-Enein, Morsy M. Abou-Sekkina, Nagy M. Khalil, Osama A. Shalma, Microstructure and refractory properties of spinel containing castables, Ceramics International 36 (2010) 1711–1717.
[5] H. Sarpoolaky, S. Zhang, W.E. Lee, Corrosion of high alumina and near stoichiometric spinels in iron-containing silicate slags, Journal of the European Ceramic Society 23 (2003) 293–300.

[6] Nagy M.A Khalil, S.A.S. El-Hemaly, Lamey G. Girgis, Aluminous cements containing magnesium aluminate spinel from Egyptian dolomite, Ceramics International 27 (2001) 865–873.
[7] A.E. Lavat, M.C. Grasselli, E.G. Lovecchio, Effect of α and γ polymorphs of alumina on the preparation of $MgAl_2O_4$-spinel-containing refractory cements, Ceramics International 36 (2010) 15–21.
[8] G.Q. Xiao, Y.Q. Gao, F. Duan, Preparation and corrosion resistance of aluminous cement containing magnesium aluminate spinel, Journal of Chinese Ceramic Society 36 (2008) 1172–1177.
[9] J.D. Cox, J.H. Sharp, The use of admixtures with calcium aluminate cements, in: Proceedings of the Conchem International Conference, Karlsruhe, Germany, 1994, p. 381.
[10] T. Knudsen, in: Proceedings of the 7th International Congress on the Chemistry of Cement, Paris, 1980, p. 170.
[11] E. Sakai, M. Daimon, R. Kondo, in: Proceedings of the 7th International Congress on the Chemistry of Cement, Paris, 1980, p. 203.